Multi-Spectral Imaging of Vegetation for Detecting CO$_2$ Leaking from Underground

Joshua H. Rouse,[1,2] Joseph A. Shaw,[1] Rick L. Lawrence,[3] Jennifer L. Lewicki,[4] Laura M. Dobeck,[5] Kevin S. Repasky,[1] Lee H. Spangler[5]

[1]*Electrical and Computer Engineering Department, Montana State University, Bozeman, MT 59717*
[2]*ITT Space Systems Division, Rochester, NY 14606 (current affiliation)*
[3]*Land Resources and Environmental Sciences Department, Montana State University, Bozeman, MT 59717*
[4]*Lawrence Berkeley National Laboratory, Earth Sciences Division, Berkeley, CA*
[5]*Chemistry and Biochemistry Department, Montana State University, Bozeman, MT 59717*

Phone: 406-994-7261

Fax: 406-994-5958

Email: jshaw@ece.montana.edu

www.coe.montana.edu/ee/jshaw

Practical geologic CO$_2$ sequestration will require long-term monitoring for detection of possible leakage back into the atmosphere. One potential monitoring method is multi-spectral imaging of vegetation reflectance to detect leakage through CO$_2$-induced plant stress. A multi-spectral imaging system was used to simultaneously record green, red, and near-infrared (NIR) images with a real-time reflectance calibration from a 3-meter-tall platform, viewing vegetation near shallow subsurface CO$_2$ releases during summer 2007 and summer 2008 at the Zero Emissions Research and Technology (ZERT) field site in Bozeman, Montana. Regression analysis of the band reflectances and the Normalized Difference Vegetation Index (NDVI) with time shows significant correlation with distance from the CO$_2$ well, indicating the viability of this method to monitor for CO$_2$ leakage. The 2007 data show rapid plant vigor degradation at high CO$_2$ levels next to the well and slight nourishment at lower, but above-background CO$_2$ concentrations. Results from the second year also show that the stress response of vegetation is strongly linked to the CO$_2$ sink-source relationship and vegetation density. The data also show short-term effects of rain and hail. The real-time calibrated imaging system successfully obtained data in an autonomous mode during all sky and daytime illumination conditions.

NDVI: Normalized Difference Vegetation Index; ZERT: Zero Emissions Research and Technology

1

Introduction

The increased consideration of geological sequestration for reducing greenhouse gas emissions is accompanied by a need for methods to detect CO_2 if it leaks from the ground into the atmosphere. Leakage of CO_2 from the ground into the atmosphere (referred to as 'seepage' by Oldenburg and Unger [2003]) not only represents compromised security of the sequestration facility, but also can result in health, safety, and environmental risks, including asphyxiation of humans or animals (Oldenburg et al., 2003). Whereas relatively low leak rates do not create immediate health or safety risks, they still require detection because of the significant amounts of gas that could potentially escape over a long time period (Oldenburg et al., 2003).

Within a broad class of optical remote sensing techniques, measurements can be made to directly detect the CO_2 gas through optical absorption (Sakaizawa et al., 2009; Humphries et al., 2008; Repasky et al., 2006; Koch et al., 2004; and Cremers et al., 2001). Alternatively, it might be possible to detect the gas indirectly through changes in the reflectance spectrum of vegetation. An extreme natural example of this occurred at Mammoth Mountain, California, where large amounts of escaping CO_2 killed wide swaths of forest vegetation (Lewicki et al., 2007a; Farrar et al., 1999; and Farrar et al., 1995). Extensive studies of the tree kill at Mammoth Mountain have demonstrated the utility of satellite, airborne, and ground-based multispectral and hyperspectral remote sensing for detecting high rates of CO_2 leakage indirectly through vegetation reflectance measurements (Martini and Silver, 2002; Martini et al.,2000; and Farrar et al.,1999).

The use of passive hyperspectral vegetation sensing for early detection and spatial mapping of CO_2 leaks from underground storage facilities was formally proposed by Pickles and Cover (2004). More recently, a hyperspectral scanning imager was used with decision-tree data analysis to detect CO_2 leakage (Keith et al., 2009) in a 2007 subsurface CO_2 release (Lewicki et al. 2009, 2007b) at the Zero Emissions Research and Technology (ZERT) field site at Montana State University in Bozeman, Montana (Spangler et al., this issue, Lewicki et al., 2007b). A portable hyperspectral sensor also was used to detect changes in vegetation reflectance spectra correlated with CO_2 leakage from the ZERT subsurface releases in 2007 and 2008 (Male et al., this issue).

Leakage detection with passive spectral imaging is based on detection of plant stress caused by elevated soil CO_2 concentration. Whereas slightly elevated CO_2 concentrations in the atmosphere can increase plant health and growth (Rogers et al., 1994; Kimball et al., 1993; and Bazzaz and Fajer, 1992), high concentrations of CO_2 in the root zone can kill plants through asphyxiation (Qi et al., 1994) and soil acidification (McGee and Gerlach, 1998). The CO_2 concentration for air inside soil under typical conditions is only several percent (concentration at 0.5 m depth), and when this concentration becomes greater than about 10 to 20 percent, root development in plants is suppressed (Farrar et al., 1999). This produces decreased uptake of water and other nutrients, leading to stress or ultimately death of the plants. The root-zone concentration of CO_2 required to kill vegetation varies with exposure time, soil moisture, soil nutrient content, and plant species. Vegetation at Mammoth Mountain was observed to exhibit stress when the soil CO_2 concentration rose to 20 percent or greater (Farrar et al., 1999).

This paper presents results of a study using multispectral imaging to detect changes in the spectral reflectance of vegetation that are correlated with proximity to the subsurface CO_2 release region. The method described here provides detection with a system that is potentially simpler and lower cost than hyperspectral imaging, and that provides continuous daytime operation in clear and cloudy weather through the use of real-time calibration using a reflectance panel deployed in the field with the imager. The use of a platform-mounted imager has demonstrated the potential of a remotely deployed instrument that avoids the need of airborne or satellite imagery and provides much higher spatial resolution, although at the expense of reduced overall spatial coverage.

The balance of this paper is organized as follows. The methodology is described, including a description of the imaging system, its calibration, its continuous outdoor deployment at the ZERT field site in Bozeman, Montana during shallow subsurface CO_2 releases in the summers of 2007 and 2008, and the data processing. Next the results of a statistical study are shown, focusing on a regression analysis of the green, red, and near-infrared reflectances and the Normalized Difference Vegetation Index (NDVI) over time. Finally, the significance and implications of the results are discussed and the paper is concluded with suggestions for future work.

Methodology

Experimental layout

During the summers of 2007 and 2008, shallow subsurface CO_2 release experiments were conducted at the ZERT site located just west of Montana State University in Bozeman, Montana, at 45.66°N., 111.08°W. (Spangler et al., this issue). Two vegetation test strips, one mown and one unmown, were oriented perpendicular to a 100-m-long, perforated pipe buried approximately 1.3-2.5 m below land surface to simulate homogeneous leakage from a horizontal well (Spangler, 2009; Lewicki et al., 2007b), as indicated in Fig. 1. The CO_2 release rates were 0.1 tons/day in the 2007 experiment (9 July – 23 July) and 0.3 tons/day in the 2008 experiment (7 July – 7 August). Both releases produced five to six "hot spots" of elevated soil CO_2 flux aligned along the surface trace of the horizontal well (e.g., Figure 1 in Lewicki et al., 2007b; Lewicki et al., this issue). We assumed that the measured CO_2 flux had positive correlation with CO_2 concentration.

Multispectral images of the vegetation test strips were obtained both before and after the releases in both years. As shown in Figs. 2 and 3, the imager was placed on a 3-m-high platform, pointed downward at a 45° angle below the horizon to view both vegetation strips from 10 m northwest of the pipe to 0.5 m northwest of the pipe in 2007, and from 10 m northwest of the pipe to 1 m southeast of the pipe in 2008. Multi-spectral imager data were analyzed in three regions, with region 1 nearest the horizontal well, region 2 in the middle, and region 3 located farthest from the well (these regions are indicated by the numbered white boxes in Fig. 1 and also marked on the photograph in Fig. 3).
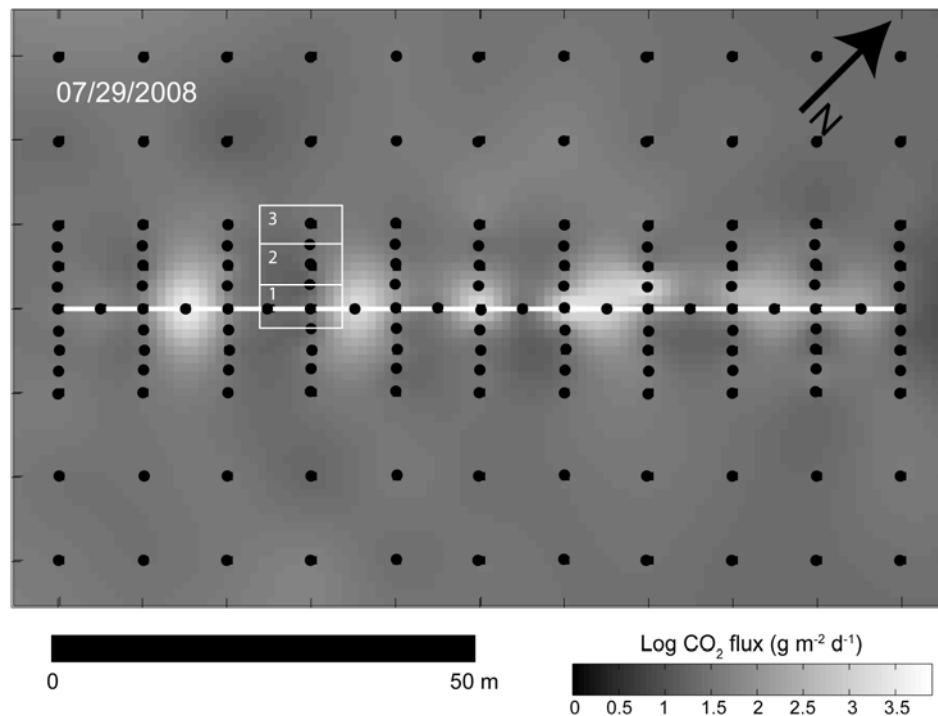
Fig. 1. CO_2 flux map interpolated based on measurements made at the black dots for the 2008 release experiment at the ZERT facility in Bozeman, Montana (Lewicki et al., this issue). The inset box indicates the approximate area observed by the multispectral imager within the vegetation test area, divided into three test regions (near, middle, and far relative to the well location). The white line indicates the surface trace of the buried CO_2 release pipe.
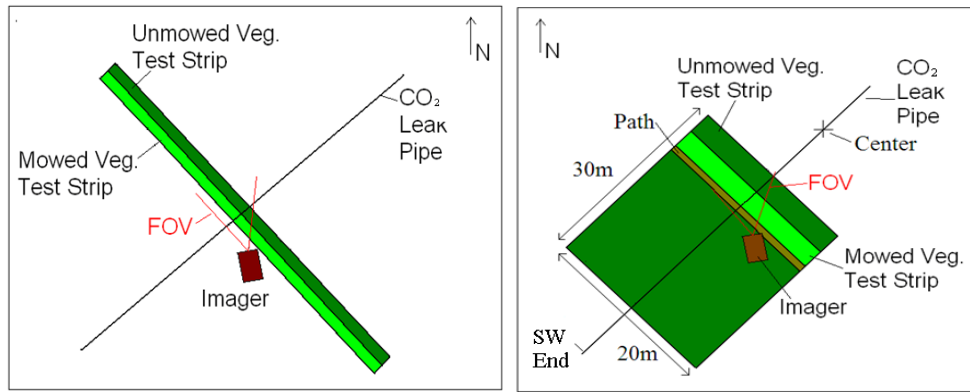
Fig. 2. Layout of the mown and unmown vegetation test segments and the multispectral imager during the 2007 (left) and 2008 (right) CO_2 release experiments. The 55° full-angle imager field of view (FOV) is indicated by the red lines.
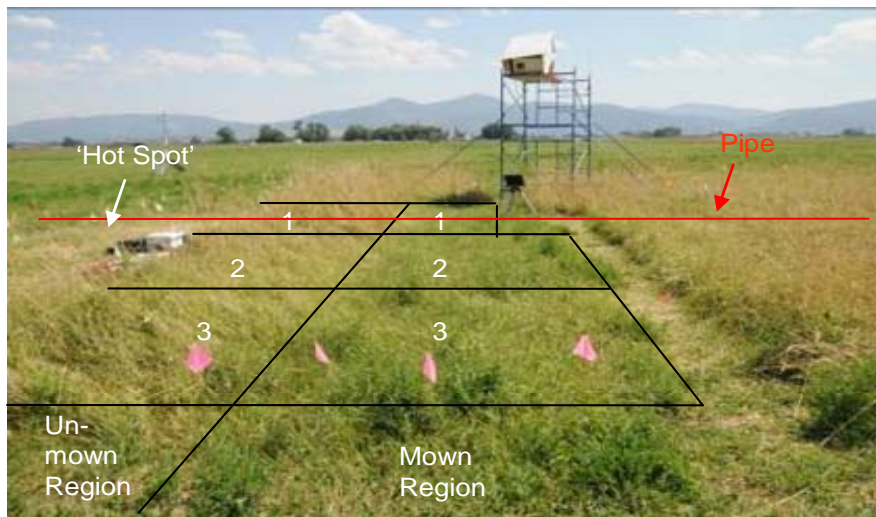
Fig. 3. Layout of the three test regions within the mown and unmown segments of the vegetation test strip. The horizontal red line indicates the sub-surface pipe from which gas was released and the "hot spot" label indicates a location of particularly high CO_2 flux, as indicated also in Fig. 1 (J. Shaw photo).

A portion of the vegetation test strip was mowed several weeks before the release started and therefore remained free of tall grass that senesced more rapidly than the underlying grasses and plants. Conversely, by the end of the experiment, the underlying vegetation in the unmown segment could only be seen by imaging through a veil of tall, mostly dead grass. This distinct difference can be seen in Fig. 3 and also in the photographs shown in Fig. 4, which were taken near the beginning and end of the 2008 release experiment. The red and blue circles on the right-hand side of Fig. 4 indicate the approximate locations of two individual plants we report on later.

For data analysis, the mown and unmown segments were both divided into three regions at progressively greater distance from the pipe, as shown in Figs. 1 and 3. Region 1 was near the pipe in 2007 (0.5 m from the pipe at closest approach) and directly over the pipe in 2008. Regions 2 and 3 were each 4.5 m long. Regions 1 and 2 were used as test areas and region 3 was the control, since its location farthest from the pipe was expected to provide a background reading unaffected by the leaking CO_2.

4

(a)   (b)
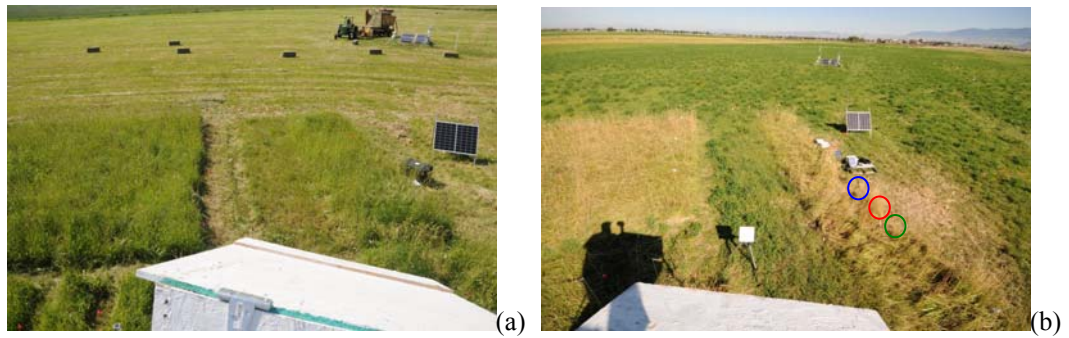
Fig. 4. Photographs of the vegetation test area taken from atop the multispectral imager platform on (a) 3 July 2008 and (b) 9 August 2008 to visually illustrate the changes in the condition of the vegetation in the mown (center) and unmown (right) segments of the test area (J. Shaw photos). The colored circles in (b) indicate the approximate locations of three individual plants discussed later.

Multispectral imaging system and calibration

The experiments used a three-chip multispectral imager (model MS3100 from Geospatial Systems, Inc.) with customized wide-angle optics. Images were calibrated to obtain spectral band-averaged reflectances by periodically viewing a photographic grey card in 2007 and by continuously viewing a Spectralon reflectance panel in 2008. The camera splits incoming light via prisms and dichroic surfaces into green (500-580 nm), red (630-710 nm), and near-infrared (NIR, 735-865 nm) bands that approximately match the corresponding Landsat satellite bands. Each of the three detector arrays are 7.6 mm × 6.2 mm with a pixel size of 4.65 μm × 4.65 μm, which results in 1392 × 1040 pixels in each image. Owing to the small detector array size, a fisheye lens adapter was added to a 20-mm f/2.8 Nikkor lens to increase the full-angle horizontal field of view from 24° to 55°. The imaging system was operated in 8-bit mode, giving 256 digital numbers (DN) for each pixel. In 2008, a computer program was employed to adjust the camera's integration time to achieve real-time exposure control based on the brightness of the pixels that were continually viewing a Spectralon reflectance calibration panel in one portion of the image.

Rigorous characterization and calibration of the entire imaging system was performed prior to deployment in the field (Rouse, 2008). Parameters that were characterized included DN vs. integration time, DN vs. gain, DN vs. f/number, DN vs. radiance, DN vs. camera temperature, DN vs. polarization angle, pixel bleeding during readout, pixel recovery when viewing a dim scene after a bright one, and spatial non-uniformity of the camera response. For the characterizations, the imager was operated looking into an integrating sphere to ensure spatially uniform radiance across the camera's field of view. Under test conditions that simulated the expected field conditions the imager stayed within a highly linear operating range; the only characteristic that required correction was the spatial non-uniformity, partly a result of the ultra-wide-angle optics used to increase the field of view. When the imager viewed a uniformly illuminated reflectance panel, there was a nearly 50 percent fall off of brightness from the center to the edge of the image. To correct this, a unique linear signal-dependent calibration function was applied to each pixel of each detector array. Gain and offset terms were found for each of these calibration functions from a linear fit to five images: one dark image, images of 50 percent and 99 percent reflectance panels illuminated by direct sunlight, and images of the same two panels illuminated by diffuse shaded skylight.

Each non-uniformity-adjusted vegetation image was calibrated radiometrically with a reflectance-panel image according to eq. 1. In this equation, subscript λ indicates the wavelength (color band), DN is the digital number for the pixel viewing the indicated object, and ρ is the reflectance (known for the calibration target, and calculated for the scene). For the 2007 experiment a nominally 18 percent reflective photographic grey card was imaged every time the imager's integration time was changed because of changes in the ambient light. In the 2008 experiment the images were calibrated by imaging a 99 percent reflective Spectralon panel that was part of every

5

image. This made it possible to calibrate each image during the experiment with higher accuracy and, coupled with the previously mentioned auto-exposure algorithm, enabled operation even in highly variable weather conditions.

$$\rho_\lambda = \left(\frac{DN_{\lambda,\text{scene}} - DN_{\lambda,\text{dark}}}{DN_{\lambda,\text{calibration target}} - DN_{\lambda,\text{dark}}} \right) * \rho_{\lambda,\text{calibration target}} \qquad (1)$$

Spectral image analysis

Calibrated reflectance data from the green, red, and NIR bands were averaged over the three regions in the mown and unmown vegetation test strips and analyzed with a linear regression technique, along with the Normalized Difference Vegetation Index (NDVI), calculated from the red and NIR bands according to eq. 2 (Rouse et al., 1974).

$$NDVI = \frac{\rho_{\text{NIR}} - \rho_{\text{red}}}{\rho_{\text{NIR}} + \rho_{\text{red}}} \qquad (2)$$

The NDVI exploits the sharp relative increase of reflectance that occurs near a wavelength of 700 nm because of strong chlorophyll absorption at visible wavelengths and high reflectance at the near infrared wavelengths related to leaf structure. As vegetation becomes stressed, its NIR reflectance falls, its red reflectance rises, and the red edge near 700 nm shifts to shorter wavelengths and becomes less steep (Horlerd, 1983; Carter, 1993; Jensen, 2000; and Carter et al., 2001). Reflectance measurements of healthy and stressed plants showed that the sensitivity of reflectance to plant stress is maximized in the 685-700 nm spectral bands (Carter, 1993; and Carter et al., 2001). These studies also showed that specific stress agents do not have spectral 'signatures,' so one should be able to detect changes in chlorophyll content, leaf anatomy, or water content by analyzing both the red and NIR portions of the spectrum, or by analyzing an index that combines these bands (Jordan, 1969; and Carter et al., 2001).

The NDVI is one particular vegetation index that combines the red and NIR band reflectances in a manner that captures the key information related to vegetation stress (Rouse et al., 1974). Experiments comparing eddy covariance measurements of ecosystem CO_2 fluxes with the NDVI measured with multispectral imaging has shown high correlation (correlation coefficient = -0.981), and that the NDVI captured the effects of changing environmental conditions such as drought, recovery, and fire on the carbon flux (Fuentes et al., 2006).

This study relies on a linear regression technique applied to time series of the imager's band reflectances and NDVI data. In addition to analyzing single spectral band reflectances and NDVI, spectral band and NDVI combinations were statistically analyzed to find the best possible combination to model vegetation stress. Time was set as the response variable, spectral bands and/or NDVI were set as predictor variables, and region number was set as the categorical variable. The full linear regression model for a general fit can be seen in eq. 3.

$$y = \beta_0 + \beta_G x_G + \beta_R x_R + \beta_{NIR} x_{NIR} + \beta_{NDVI} x_{NDVI} + \beta_\tau \tau + \beta_{G,\tau}(x_G * \tau) + \beta_{R,\tau}(x_R * \tau) +$$
$$\beta_{NIR,\tau}(x_{NIR} * \tau) + \beta_{NDVI,\tau}(x_{NDVI} * \tau) \qquad (3)$$

In eq. 3, y is the decimal date (response variable), β_0 is the y-intercept (linear regression coefficient), β_G is the slope for the green band, x_G is the green reflectance (predictor variable), β_R is the slope for the red band, x_R is the red reflectance, β_{NIR} is the slope for the NIR band, x_{NIR} is the NIR reflectance, β_{NDVI} is the slope for the NDVI, , x_{NDVI} is the computed NDVI value, β_τ is the slope for the region, τ is the region number (categorical variable), and $\beta_{G,\tau}$, $\beta_{R,\tau}$, $\beta_{NIR,\tau}$, and $\beta_{NDVI,\tau}$ are the slope terms for the interaction terms. All the β values were calculated in linear regression analysis software.

To find the best band combination, coefficients of determination (R^2) and p-values were analyzed to determine how well the regressions fit the data, if the regression was significant, and if the spectral difference in vegetation regions were statistically separable. The possible differences in the spectral combinations were explored via both the intercepts and slopes from the linear regressions; a difference in slope indicates a different vegetation response to stress and a difference in intercept most likely means that the vegetation started at different health values. The variables were selected using a stepwise regression selection procedure based on an Extra-Sum-of-Squares F-test.

Results

The regression analysis showed that the NDVI was the most consistent choice for explaining the variability in vegetation health and was strongest for statistically separating regions. A single best regression equation was used in this study (the form of which is shown in eq. 4) for analysis of each year's data and individual plants to standardize the analysis.

$$\text{Date} = \beta_0 + \left(\beta_{\text{NDVI}} \cdot \text{NDVI}\right) + \tau_{i,1-2} + \left(\tau_{s,1-2} \cdot \text{NDVI}\right) + \tau_{i,1-3} + \left(\tau_{s,1-3} \cdot \text{NDVI}\right) + \tau_{i,2-3} + \left(\tau_{s,2-3} \cdot \text{NDVI}\right) \quad (4)$$

Here, date is the response variable, β_0 is the offset, β_{NDVI} is the slope, NDVI is the predictor variable, the three τ_i variables account for differing intercepts (and therefore different starting conditions among regions), while the three τ_s variables account for the different slopes (and therefore rates of response) among the regions.

The NDVI was most consistent in that it had the highest R^2 values for both the 2007 and 2008 un-mown segments, but had slightly lower values (by less than 0.065) than combinations of red-NIR and green-NIR-NDVI for the mown segments and the individual plants, respectively. More importantly, the NDVI alone was best able to statistically separate vegetation regions in every case. The NDVI allows more effective modeling of interactions between spectral responses and regions, although spectral band combinations are best for explaining variability in the reflectance spectrum itself (Maynard et al., 2006; Lawrence and Ripple, 1998).

After exploring various combinations of band reflectances and NDVI, linear regressions only involving NDVI were used, even though according to Robinson (2004) a regression involving a spectral band interaction term (such as NDVI, which involves both NIR and red reflectances) without the individual bands is not statistically ideal. This was done because when the band reflectances were included, the ability of the regression to statistically separate regions and the significance of each of the bands and NDVI towards the regression were diminished. It was also found from the 2007 and 2008 field experiments that the use of a robust calibration technique increases the accuracy of a plant stress detection system, enough that the effects of a small increase in CO_2 concentration, rain, and hail are all detectable, even in cloudy conditions.

In the rest of this section, results are shown in the form of tables and graphs of regression parameters and lines plotted with the measured data. This is done separately for the mown and unmown segments of the vegetation test area for both the 2007 and 2008 experiments. Although the regressions were calculated as time-versus-NDVI (or reflectance), we plot the results with time on the abscissa to simplify physical understanding of the temporal evolution. These results are interpreted and discussed further in the next section of the paper.

2007 Experiment Results

The 2007 experiment resulted in a limited amount of useful data because of calibration difficulties caused by an unexpectedly non-Lambertian grey card reflectance (some grey cards were found to be quite Lambertian, while others were found to be highly specular). Even still, images selected with the grey card held at the proper angle gave a sufficiently diffuse, approximately 18 percent reflection that provided a usable calibration for the imager. NDVI data obtained from image regions that should be separable did turn out to be statistically separable (p-value less than 0.05) with high coefficients of determination (R^2), from 0.4472 to 0.7256.
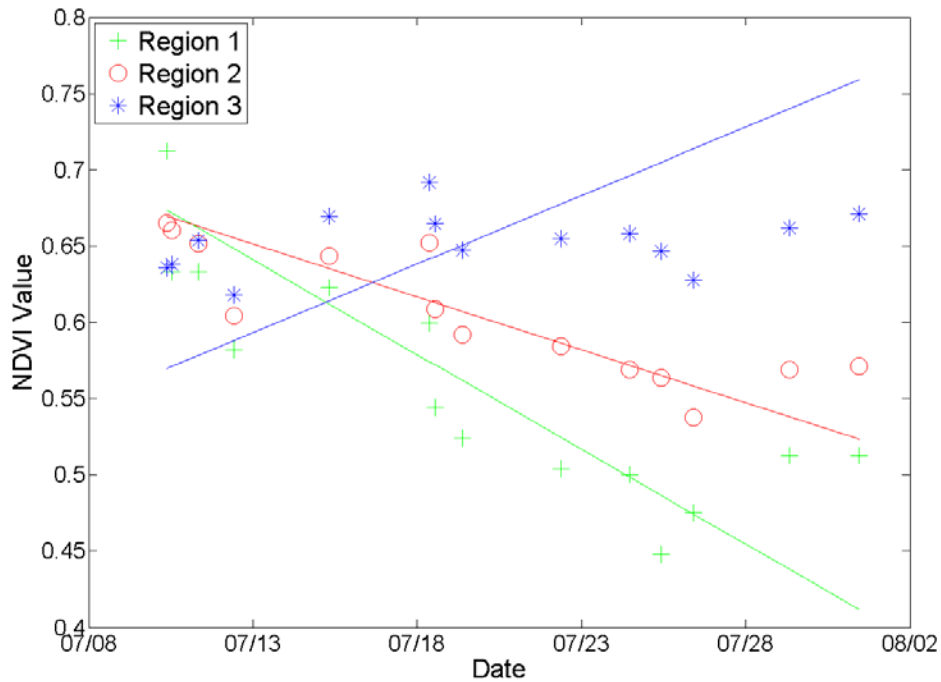
7

2007 results for the mown segment

Results from the application of the previously described statistical analysis to 2007 mown-segment data are shown in tables and graphs in this subsection. Table 1 lists the R^2 and p-values that indicate moderately high correlation of the NDVI and time (used as the response variable). Table 2 lists the p-values that distinguish between regions at different distance from the buried pipe. The data and resulting regression lines for mown-segment 2007 data are shown graphically in Fig. 5. This graph shows the trend of weaker plant stress in region 2 relative to region 1 (nearest the pipe), measured by the change in NDVI over time during the CO_2 release, although these differences were marginally significant and not significant at $\alpha = 0.05$. The blue regression line for region 3 appears skewed because of the lack of variability of NDVI over time in this control region located farthest from the pipe and both regions 1 and 2 were statistically significantly different than region 3 ($\alpha = 0.05$).

Table 1: 2007 mown segment date-versus-NDVI regression R^2 and p-values.

	Regression R^2	Regression p-Value
NDVI	0.45	<0.01

Table 2: 2007 mown segment date-versus-NDVI regression p-values that distinguish between vegetation regions.

	p-Value		
	Regions 1, 2	Regions 2, 3	Regions 1, 3
Intercept Term	0.074749	0.00443	0.023617
Slope Term	0.108908	0.00345	0.017171

Fig. 5. Plot of 2007 mown-segment date-versus-NDVI regression lines and measured data for regions 1 (green), 2 (red), and 3 (blue).

8

## 2007 results for the unmown segment

Results of the statistical analysis applied to 2007 data in the unmown segment are shown in tables and graphs in this subsection. Table 3 lists the R^2 and p-values that indicate high correlation of the NDVI and time (the response variable). Table 4 lists the p-values that distinguish between regions at different distance from the buried pipe. The data and resulting regression lines for 2007 data in the unmown segment are shown graphically in Fig. 6. This graph again shows the trend of weaker plant stress in region 2 relative to region 1 (nearest the pipe), measured by the change in NDVI over time during the CO_2 release. Differences between regions 1 and 2 again were marginally significant, while differences between regions 1 and 3 were significant, although regions 2 and 3 were not significantly different.

Table 3: 2007 unmown segment date-versus-NDVI regression R^2 and p-values.

	Regression R^2	Regression p-value
NDVI	0.73	<0.01

Table 4: 2007 unmown segment date-versus-NDVI regression p-values that distinguish between vegetation regions.

	p-Value		
	Regions 1, 2	Regions 2, 3	Regions 1, 3
Intercept Term	0.1017	0.2908	0.0157
Slope Term	0.0986	0.3432	0.0187
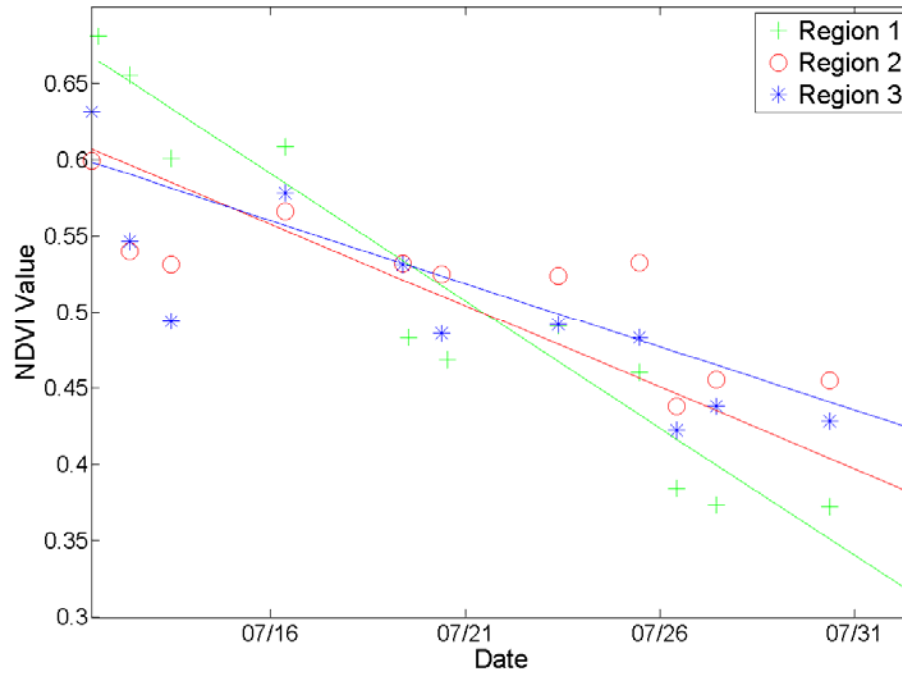
Fig. 6. Plot of 2007 unmown segment date-versus-NDVI regression lines and measured data for regions 1 (green), 2 (red), and 3 (blue).

2008 Experiment Results

In the 2008 experiment, better calibration techniques led to good data being collected every day the system was operated correctly. NDVI data obtained from image regions that should be separable did, in fact, turn out to be statistically separable (p-value less than 0.05) with high coefficients of determination (R^2). For the 2008 data, the date-versus-NDVI regression plots include horizontal green and red lines to indicate the beginning and end of the gas release, respectively. Similarly, rain events are indicated with dashed black horizontal lines and hail events are shown as solid black horizontal lines.

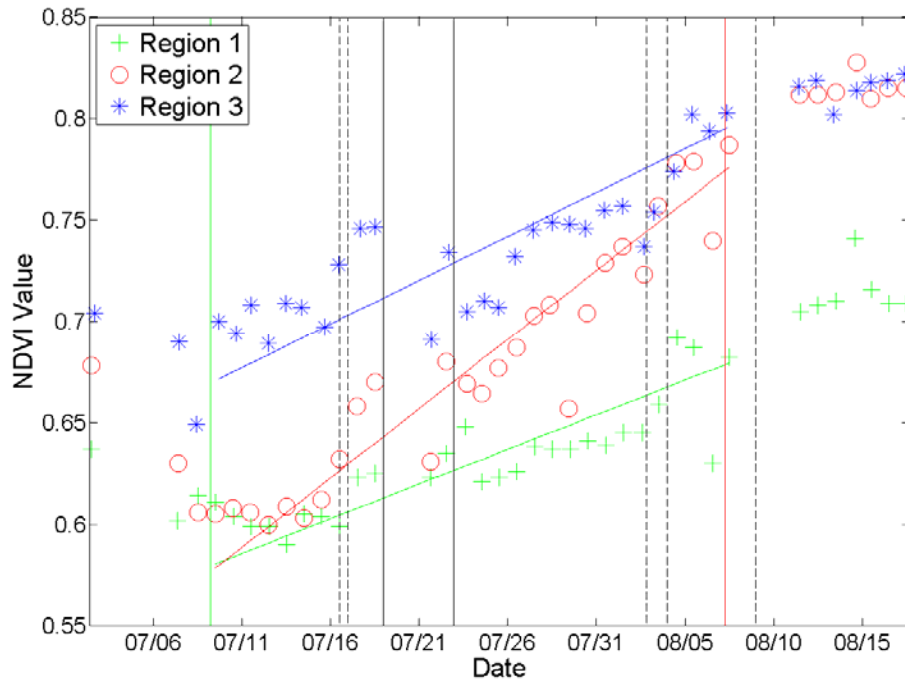### *2008 results for the mown segment*

Results of the statistical analysis applied to 2008 data in the mown segment are shown in tables and graphs in this subsection. Table 5 lists the R^2 and p-values that indicate high correlation of the NDVI and time (the response variable). Table 6 lists the p-values that distinguish between regions at different distance from the buried pipe. The data and resulting regression lines for 2008 data in the mown segment are shown graphically in Fig. 7. This graph shows a trend of increasing plant vigor throughout the release experiment. However, the rate of increase is lower in regions 1 relative to region 2, while regions 1 and 3 are not statistically different in this case, compatible with the hypothesis that higher CO_2 flux in region 1 (near the release pipe; Fig. 1) was inhibiting plant vigor relative to the gains made in region 2. Plant vigor also is correlated with frequent and heavy rain events (Fig. 7).

Table 5. 2008 mown segment date-versus-NDVI regression R^2 and p-values.

	Regression R^2	Regression p-value
NDVI	0.73	<0.01

Table 6. 2008 mown segment date-versus-NDVI regression p-values that distinguish between vegetation regions.

	p-Value		
	Regions 1, 2	Regions 2, 3	Regions 1, 3
Intercept Term	0.000881	0.00436	0.604922
Slope Term	0.000305	0.01291	0.172055

Fig. 7. 2008 mown segment date-versus-NDVI regression lines and measured data for regions 1 (green), 2 (red), and 3 (blue). The start and end of the CO_2 release are marked by the vertical green and red line lines. Rain events are marked by vertical black dashed lines and hail events are marked by vertical black solid lines.
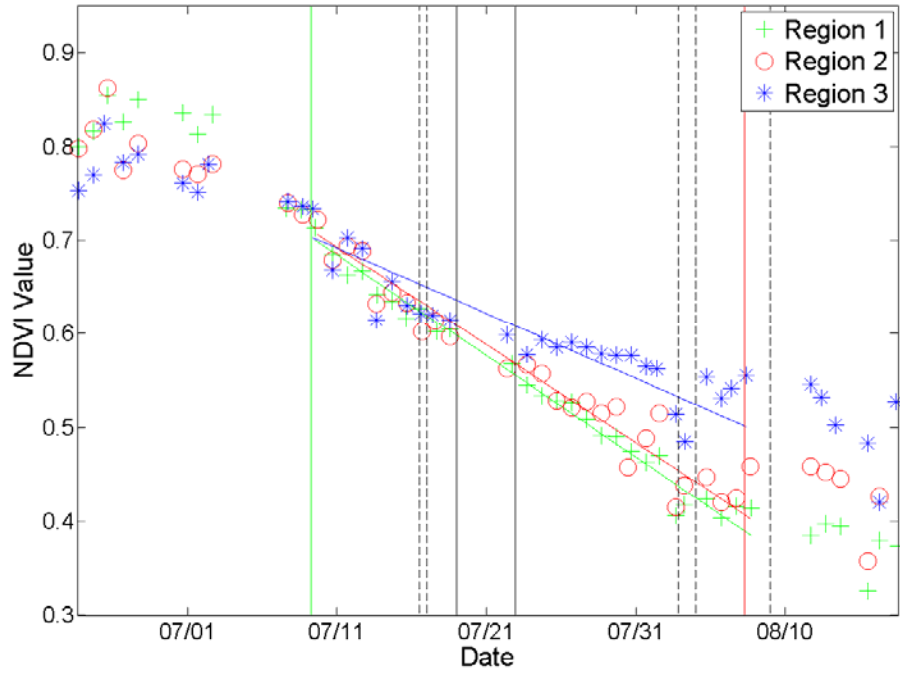
2008 results for the unmown segment

Results of the statistical analysis applied to 2008 data in the unmown segment are shown in tables and graphs in this subsection. Table 7 lists the R^2 and p-values that indicate very high correlation of the NDVI and time (the response variable). Table 8 lists the p-values that distinguish between regions at different distance from the buried pipe. The data and resulting regression lines for 2008 data in the unmown segment are shown graphically in Fig. 8. In contrast to the increasing plant vigor observed over time in the mown segment, this figure indicates a steady decrease of vigor (increase of plant stress) over the course of the 2008 release experiment. This difference can be understood by observing the veil of tall, senesced prairie grass that partially obscures the imager's view to the relatively healthy underlying vegetation, as is seen in the photographs of Fig. 3. Despite this veil of senesced tall grass, the NDVI still indicates a higher rate of increased plant stress in region 1 (near the pipe) relative to regions 2 and 3 (but essentially indistinguishable rates between regions 1 and 2).

Table 7. 2008 unmown segment date versus NDVI regression R^2 and p-values.

	Regression R^2	Regression p-value
NDVI	0.9	<0.01

11

Table 8. 2008 unmown segment date versus NDVI regression *p*-values that distinguish between vegetation regions.

	p-Value		
	Regions 1, 2	Regions 2, 3	Regions 1, 3
Intercept Term	0.538	6.32E-06	8.33E-07
Slope Term	0.721	8.36E-05	2.59E-05

Fig. 8. 2008 unmown segment date-versus-NDVI regression lines and measured data for regions 1 (green), 2 (red), and 3 (blue). Vertical lines indicate start (green), stop (red), rain (black dashed), and hail (black solid), as in Fig. 7.

## *2008 results for individual plants within unmown segment*

The same statistical analysis also was applied to 2008 data at the locations of three individual plants that had been observed closely with a hand-held hyperspectral sensor (Male et al., this issue). This was done to assess the ability of the platform-mounted multispectral imager to monitor detail at the single-plant level. The results for these three individual plants are shown in this subsection. Table 9 lists the R^2 and *p*-values that indicate high correlation of the NDVI and time (the response variable) for these individual plants. Table 10 lists the *p*-values that distinguish between individual plants and the unmown region 3. The data and resulting regression lines for the individual plants are shown graphically in Fig. 9. The stress for all three plants increased at similar rates during the period of the release, but stopped increasing almost immediately after the CO_2 stopped flowing.

Table 9. Individual plants' date-versus-NDVI regression R^2 and *p*-values.

	Regression R^2	Regression *p*-value
NDVI	0.74	<0.01

12

Table 10. Individual plants' date-versus-NDVI regression *p*-values that distinguish between individual plants and the unmown region 3.

	p-Value (specific plant compared to 2008 unmown region 3)		
	Plant 8	Plant 9	Plant 10
Intercept Term	0.00651	9.68E-05	7.45E-06
Slope Term	0.004116	0.000353	0.00125
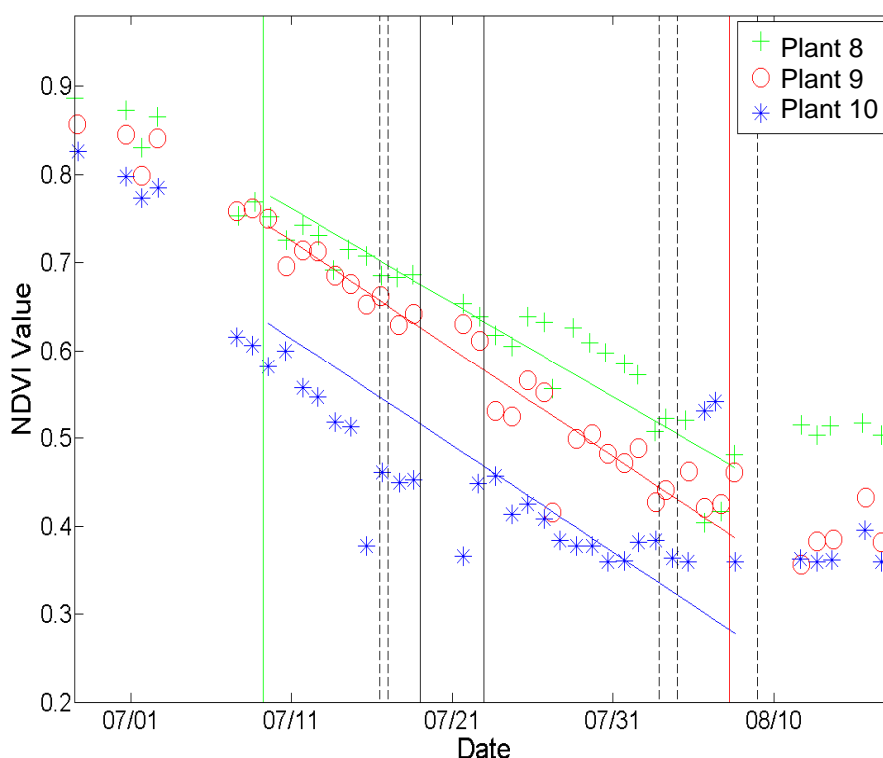
Fig. 9. 2008 individual plant date-versus-NDVI regression lines and measured data for the unmown segment. Plant locations are adjacent to hot spot, as indicated approximately with colored circles in Fig. 4b. Vertical lines are the same as in Figs. 7 and 8.

Discussion

The data obtained during the 2007 and 2008 release experiments indicate the ability of a multispectral imaging system to detect plant stress or nourishment that is correlated with increased CO_2 concentrations resulting from a simulated leak. Results from both 2007 and 2008 are consistent with the hypothesis that elevated CO_2 flux in region 1 (near the pipe) leads to increased plant stress that manifests itself as a higher rate of decay or lower rate of increase in the NDVI. With increased CO_2 levels, and depending on sink-source balance, there is a noticeable increased stress or decrease in plant vigor. The connection between NDVI and CO_2 levels is supported further by the logarithmic map of CO_2 flux measured at the ZERT field site during the 2008 release experiment (Lewicki et al., this issue), which is shown in Fig. 1. The east side of the vegetation test area is on the edge of a hot spot where the vegetation was entirely dead within several weeks of the beginning of the release. Overall, the CO_2 flux is above background levels in

13

the eastern areas of regions 1 and 2 (within about 5 m of the release pipe) and at background levels in region 3.

Owing to a veil of tall, senesced prairie grass obscuring a clear view of the underlying vegetation (see Fig. 3), the stress signatures were suppressed in the data for the unmown segment. Nevertheless, there was statistically significant separation of the regression lines for regions 1 and 2 relative to region 3 (Fig. 8). Ongoing studies are exploring this further through higher-spatial-resolution processing of multispectral imager data.

For the 2008 experiment, soil moisture and precipitation data were also available to help determine how the change in plant health was driven by rain and hail events. Although the regression results show that the overall NDVI trends are highly correlated with increased CO_2 fluxes, short-term effects of rain and hail also can be seen as short-term correlated fluctuations in rain, soil moisture, and measured NDVI. As indicated in the plot of soil moisture data vs. time shown in Fig. 10, there was generally a drying trend, punctuated by large short-term increases in soil moisture after rain and hail events that actually resulted in the net change being slightly positive (i.e., the soil moisture at the end of the release was slightly higher than at the beginning of the release). The net increase of soil moisture throughout the release suggests that the stress seen in the NDVI plots is not caused primarily by a lack of soil moisture, although there are other factors that also need to be explored in future studies. In agreement with arguments about sink-source importance (Arp, 1991), the dense vegetation in the unmown segment had to compete more than the vegetation in the mown segment, shown by smaller relative changes in soil moisture, thereby allowing the mown segment to become healthier.

It is useful to note that the improved calibration and operation methods in the 2008 experiment made it possible to see effects of rain and hail in the multispectral data. The NDVI plots show rain events as dashed black lines and hail events as solid black lines. These plots, along with the precipitation and soil moisture data (shown in Fig. 10), show that directly after a hail storm the vegetation NDVI decreases, but as the water saturates the ground and the moisture is taken in by the vegetation, within a day or two the detectable plant vigor increases. This increase in vigor can also be seen immediately after significant rainfalls without hail (dashed horizontal lines).
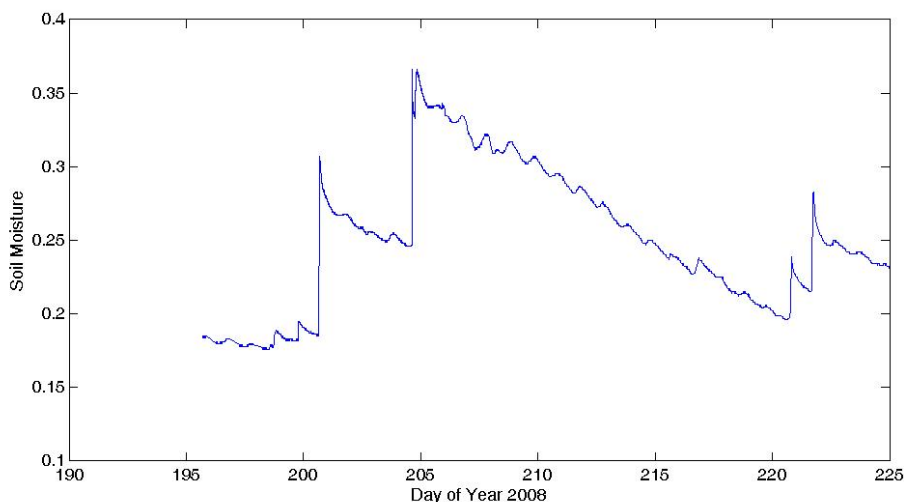
Fig. 10. Time-series plot of volumetric soil moisture near the vegetation test area during the 2008 release experiment. The general drying trend was offset by significant periodic rainfall, which led to the soil moisture being comparable at the beginning (7 July 2008 = day 189) and end (7 Aug 2008 = day 220) of the release.

Conclusions

A platform-mounted multispectral imager detected statistically significant changes in the reflectance spectra of vegetation that is strongly correlated with leaking CO_2. This was shown by

14

linking increased CO_2 concentration with plant stress or nourishment, ruling out the effects of water, considering sink-source balance, and using NDVI to show that regions of stressed vegetation and regions of non-stressed vegetation are statistically separable.

The multispectral imager was run in a mostly autonomous mode, in both clear and cloudy conditions, whereas some other sensors require sustained periods of clear skies to operate reliably. This was made possible by placing the imager in a weatherproof box and by placing a high-quality reflectance calibration target in the field of view of the imager so that it is imaged along with the vegetation in every image. The robust calibration and continuous operating mode also allowed finer-scale, short-term effects caused by rain and hail to be observed in the data.

It was found that this system was best able to detect stress effects from the CO_2 leak when the vegetation region in question was left unmown. This is because of the competing sink-source relationship between densely and less densely packed vegetation. When the vegetation is left in its natural state, there will be a higher density of vegetation, and drying during warm summer months will create more competition for water, thereby throwing off the sink-source relationship and enhancing the effects from CO_2. The CO_2 effects can still be observed in the mown segment, but the correlation was stronger for the unmown segment data.

This study suggests that future work is warranted to produce an even lower-cost system that can operate autonomously for robust multispectral vegetation stress detection. Such a system with sufficiently low cost could be reproduced to, for example, sample multiple portions of a large area overlying a sequestration facility. Work is ongoing at Montana State University to develop and test exactly such a system, using a low-cost camera with a filter wheel, custom wide-angle optics, and integrated microcontroller for data acquisition.

References

Arp, JW (1991) Effects of source-sink relations on photosynthetic acclimation to elevated CO_2, Plant, Cell, Environ., 14:869-875.

Bazzaz FA, Fajer ED (1992) Plant life in a CO_2-rich world. Sci. Am. 266:68-74).

Carter GA (1993) Responses of Leaf Spectral Reflectance to Plant Stress. Am. J. Botany 80:239-243.

Carter GA, Knapp AK (2001) Leaf optical properties in higher plants: linking spectral characteristics to stress and chlorophyll concentration. Am. J. Botany 88:677–684.

Cremers DA, Ebinger MH, Breshears DD, Unkefer PJ, Kammerdiener SA, Ferris MJ, Catlett KM, Brown JR (2001) Measuring total soil carbon with laser-induced breakdown spectroscopy (LIBS). J. Environ. Quality 30:2202-2206.

Farrar CD, Neil JM, Howle JF (1999) Magmatic carbon dioxide emissions at Mammoth Mountain, California. U.S. Geological Survey Water-Resources Investigations Report 98-4217.

Farrar CD, Sorey ML, Evans WC, Howle JF, Kerr BD, Kennedy BM, King C-Y, Southon JR (1995) Forest-killing diffuse CO_2 emission at Mammoth Mountain as a sign of magmatic unrest. Nature 376:675-678.

Fuentes DA et al. (2006) Mapping carbon and water vapor fluxes in a chaparral ecosystem using vegetation indices derived from AVIRIS. Remote sens. Environ. 103:312-323.

Horlerd, NH, Dockraya M, Barber J (1983) The red edge of plant leaf reflectance. Int. J. Remote Sens. 4:273-288.

Humphries SD, Nehrir AR, Keith CJ, Repasky KS, Dobeck LM, Carlsten JL, Spangler LH (2008) Testing carbon sequestration site monitor instruments using a controlled carbon dioxide release facility. Appl. Opt. 47:548-555.

Jensen, JR (2000) Remote Sensing of the Environment: An Earth Resource Perspective. Prentice-Hall, Upper Saddle River, NJ.

Jordan, CF (1969) Derivation of Leaf-Area Index from Quality of Light on the Forest Floor. Ecology 50:663-666.

Keith CJ, Repasky KS, Lawrence RL, Jay SC, Carlsten JL (2009) Monitoring effects of a controlled subsurface carbon dioxide release on vegetation using a hyperspectral imager. Int. J. Greenhouse Gas Control 3:626-632.

Kimball BA, Mauney JR, Nakayama FS, Idso SB (1993) Effects of increasing atmospheric CO_2 on vegetation. Plant Ecology 104/105:65-75.

Koch GJ, Barnes BW, Petros M, Beyon JY, Amzajerdian F, Yu J, Davis RE, Ismail S, Vay S, Kavaya MJ, Singh UN (2004) Coherent differential absorption lidar measurements of CO_2. Appl. Opt. 43:5092-5099. doi:10.1364/AO.43.005092.

Lawrence RL, Ripple WJ (1998) Comparisons among vegetation indices and bandwise regression in a highly disturbed, heterogeneous landscape: Mount St. Helens, Washington, Remote Sens. Environ. 64:1453-1463.

Lewicki JL, Hilley GE, Tosha T, Aoyagi R, Yamamoto K, Benson SM (2007a) Dynamic coupling of volcanic CO_2 flow and wind at the Horseshoe Lake tree kill, Mammoth Mountain, California. Geophys. Res. Let. 34:L03401, doi:10.1029/2006GL028848.

Lewicki JL, Oldenburg CM, Dobeck L, Spangler LH (2007b) Surface CO_2 leakage during two shallow subsurface CO_2 releases. Geophys. Res. Let. 34:L24402. doi:10.1029/2007/GL032047

Lewicki JL, Hilley GE, Fischer ML, Pan L, Oldenburg CM, Dobeck L, Spangler LH (2009) Eddy covariance observations of surface leakage during shallow subsurface CO_2 releases. J. Geophys. Res. 114:D12302, doi:10.1029/2008JD011297.

Lewicki JL, Hilley GE, Dobeck L, Spangler LH (this issue), Dynamics of CO_2 fluxes and concentrations during a shallow subsurface CO_2 release. Environmental Earth Sci. doi: 10.1007/s12665-009-0396-7.

Male EJ, Pickles WL, Silver EA, Hoffman GD, Lewicki JL, Apple M, Repasky KS, Burton EA (this issue) Using hyperspectral plant signatures for CO_2 leak detection during the 2008 ZERT CO_2 sequestration field experiment in Bozeman, Montana. Environmental Earth Sci. doi: 10.1007/s12665-009-0372-2.

Martini BA, Silver EA (2002) The evolution and present state of tree-kills on Mammoth Mountain, California: tracking volcanogenic CO_2 and its lethal effects. Proc. 2002 AVIRIS Airborne Geoscience Workshop, Jet Propulsion Laboratory, California Institute of Technology, Pasadena, CA.

16

Martini BA, Silver EA, Potts DC, Pickles WL (2000) Geological and geobotanical studies of Long Valley, CA, USA utilizing new 5m hyperspectral imagery. Proc. Int. Geosci. Rem. Sens. Symposium, IGARSS2000 (IEEE) 4:1376-1378, doi:10.1109/IGARSS.2000.857212.

Maynard CL, Lawrence RL, Nielsen GA, Decker G (2006) Modeling vegetation amount using bandwise regression and ecological site descriptions as an alternative to vegetation indices. GIScience and Remote Sens. 43:1-14.

McGee KA, TM Gerlach (1998) Annual cycle of magmatic CO_2 in a tree-kill soil at Mammoth Mountain, California: Implications for soil acidification. Geology 26:463-466.

Oldenburg CM, Unger AJA (2003) On leakage and seepage from geologic carbon sequestration sites: unsaturated zone attenuation. Vadose Zone J. 2:287-296.

Oldenburg CM, Lewicki JL, Hepple RP (2003) Near-surface monitoring strategies for geologic carbon dioxide storage verification, Lawrence Berkeley National Laboratory Report, LBNL-5408.

Pickles WL, Cover WA (2004) Hyperspectral geobotanical remote sensing for CO_2 storage monitoring. Lawrence Livermore National Laboratory Report UCRL-JRNL-204165.

Qi J, Marshall JD, Matson KG (1994) High soil carbon dioxide concentrations inhibit root respiration of Douglas Fir. New Phytology 128:435-441.

Repasky KS, Humphries SD, Carlsten JL (2006) Differential absorption measurements of carbon dioxide using a temperature tunable distributed feedback diode laser. Rev. Sci. Instrum. 77:113107. doi:10.1063/1.2370746.

Robinson AP, Pocewicz AL, Gessler PE (2004) A cautionary note on scaling variables that appear only in products in ordinary least squares. For. biometry, modeling inf. sciences 1:83–90

Rogers HH, Runion GB, Krupa SV (1994) Plant responses to atmospheric CO_2 enrichment with emphasis on roots and the rhizosphere. Environmental Pollution 83:155-189.

Rouse JH (2008) Measurements of plant stress in response to CO_2 using a three-CCD imager. M.S. Thesis, Dept. of Electrical and Computer Engineering, Montana State University, Bozeman, Montana USA. Available at http://etd.lib.montana.edu/etd/2008/rouse/RouseJ1208.pdf

Rouse JW, Haas RH, Scell JA, Deering DW, Harlan JC (1974) Monitoring the vernal advancement of retrogradiation of natural vegetation. NASA/GSFC Type III, 371.

Sakaizawa D, Nagasawa C, Nagai T, Abo M, Shibata Y, Nakazato M, Sakai T (2009) Development of a 1.6 μm differential absorption lidar with a quasi-phase-matching optical parametric oscillator and photon-counting detector for the vertical CO_2 profile. Appl. Opt. 48:748-757. doi:10.1364/AO.48.000748.

Spangler, LH, Dobeck LM, Repasky KS, Nehrir AR, Humphries SD, Barr JL, Keith CJ, Shaw JA, Rouse JH, Cunningham AB, Benson SM, Oldenburg CM, Lewicki JL, Wells AW, Diehl R, Strazisar BR, Fessenden JE, Rahn RA, Amonette JE, Barr JL, Pickles WL, Jacobson JD, Silver EA, Male EJ, Rauch HW, Gullickson KS, Trautz R, Kharaka Y, Birkholzer J, Wielopolski L (this issue) A shallow subsurface controlled release facility in Bozeman, Montana USA for testing near-surface CO_2 detection techniques and transport models. Environmental Earth Sci. doi: 10.1007/s12665-009-0400-2.